Climate impact on river incision on hotspot volcanoes: insights from paleotopographic reconstructions and numerical modelling

Loraine Gourbet, Sean F. Gallen, Vincent Famin, Laurent Michon, Miangaly Olivia Ramanitra, Eric Gayer

Earth Planet. Sci. Lett. 646 (2024) 118973

Contents lists available at ScienceDirect

Earth and Planetary Science Letters

journal homepage: www.elsevier.com/locate/epsl

Climate impact on river incision on hotspot volcanoes: insights from paleotopographic reconstructions and numerical modelling

Loraine Gourbet [a,b,*], Sean F. Gallen [c], Vincent Famin [a,d], Laurent Michon [a,d], Miangaly Olivia Ramanitra [a], Eric Gayer [d]

[a] Université de La Réunion, Laboratoire GéoSciences Réunion, F-97744 Saint-Denis, France
[b] Earth Surface Process Modelling, GFZ German Research Centre for Geosciences, 14473 Potsdam, Germany
[c] Department of Geosciences, Colorado State University, Fort Collins, CO, USA
[d] Université Paris-Cité, Institut de physique du globe de Paris, CNRS, UMR 7154, F-75005 Paris, France

ARTICLE INFO

Edited by: Carolina Lithgow-Bertelloni.

Keywords:
Volcanic islands
River incision
Erosion
Landscape evolution model
Climate

ABSTRACT

Climate's role in governing landscape evolution has been intensely studied for several decades, but few studies clearly document climate-landscape interactions in natural landscapes. This study aims to improve understanding of climate-landscape linkages using hotspot volcanic islands in the tropics as natural laboratories. Relatively uniform lithology, strong precipitation and climate gradients, and known initial topographic conditions on Réunion and Mauritius islands (Réunion hotspot) and Kaua'i (Hawaii hotspot) enable us to explore the impact of climate on erosion rates and geomorphic process. We reconstruct paleo-topography of drainage basins based on preserved remnants of relict topography from past volcanic events that repaved the landscapes that are differenced from the modern-day topography to determine eroded volumes. Existing geochronology of the volcanic flows allows us to constrain the timing of repaving (a proxy for the initiation of erosion) and basin average erosion rates. The initial and final conditions and the duration of erosion are used to calibrate a simple stream power model for bedrock river incision for each basin using a Bayesian inversion. We compare the erosion rate and calibrated stream power parameters to precipitation and climate data for each drainage basin on each island to explore potential relationships. Results show that basin average erosion rates for basins eroding $< \sim 1$ mm/yr show a positive relationship with mean annual precipitation (MAP) and a negative relationship with the duration of erosion. Importantly, MAP and erosion duration are correlated, so we infer that the negative correlation between erosion rate and duration is coincidental. The stream power slope exponent and erodibility coefficient only exhibit significant correlations with climate parameters for Réunion Island, particularly mean annual cyclonic precipitation. Our results demonstrate that both mean annual precipitation and extreme events control long-term landscape evolution on volcanic islands.

1. Introduction

Climate is a major driver of changes in erosion and a critical agent in landscape evolution (Molnar and England, 1990). However, the exact nature of how climate impacts erosion rates and the pace of landscape evolution remains uncertain. A major outstanding question is the role of mean precipitation versus precipitation variability on erosion. Adams et al. (2020) proposed that mean precipitation rates exert a dominant control on long-term incision rates in the Himalayas. From a theoretical point of view, however, even for the same mean annual rainfall rate, erosion rates can differ by several orders of magnitude depending on rainfall variability when erosion thresholds are important (Deal et al., 2018). Based on a global study of bedrock river basins assumed to be at steady state (i.e. where erosion balances uplift), Marder and Gallen (2023) suggested that at moderate to high erosion rates, landscapes in more humid environments have higher bulk erosional efficiency than those in arid settings. The debate is particularly vigorous in the case of volcanic islands where landscapes do not reach a steady state because the topography is episodically reset by erupted deposits covering incised relief. Carefully designed studies in natural systems have the ability to improve understanding of how climate affects landscape evolution and test existing theories of climate-driven landscape change.

* Corresponding author.
E-mail address: gourbet@gfz-potsdam.de (L. Gourbet).

https://doi.org/10.1016/j.epsl.2024.118973
Received 30 December 2023; Received in revised form 30 June 2024; Accepted 25 August 2024
Available online 20 September 2024

Volcanic islands present exceptional natural laboratories for assessing the role of climate on landscape evolution because their initial topography can be estimated by reconstructing the un-incised volcanic edifice, and it is easy to radiometrically date volcanic flows that repave landscapes (Ollier, 1988; Ferrier et al., 2013b; Gayer et al., 2021). On tropical volcanic islands, erosion is characterized by shallow landslides, flank collapses, and fluvial incision that control relief evolution. Known age and geometry of pre-erosion topography of these islands allow the calculation of long-term, time-averaged erosion rates based on excavated volumes (Salvany et al., 2012; Ferrier et al., 2013b; Gayer et al., 2021). Hotspot tropical volcanic islands lack significant tectonic activity, exhibit relatively uniform lithology, and can experience strong climate and precipitation gradients due to a combination of prevailing wind direction and orography. For example, in Réunion Island (Réunion hotspot), precipitation rates range from 500 mm/yr to 12,000 mm/yr on the leeward and windward sides, respectively. Gayer et al. (2019) showed that long-term basin-averaged erosion rates of Réunion increase with tropical cyclone-induced rainfall variability rather than mean annual rainfall. In contrast, in Kaua'i (Hawai'i hotspot), Ferrier et al. (2013a) showed that the efficiency of bedrock river incision is linearly correlated with mean annual precipitation rates. Dramatic discrepancies also exist between basin-averaged erosion rates estimated on Kaua'i (0.003 to 0.1 mm/yr; Ferrier et al., 2013b) and Réunion (0.8 to 10 mm/yr; Gayer et al., 2019), despite the similar rock types and intensity of mean annual precipitation of both islands.

This study aims to test climate parameters (precipitation rates) against long-term basin-averaged erosion rates and fluvial incision model parameters on hotspot tropical volcanic islands, in order to identify potential climate signals in their landscape evolution. We selected Réunion and Mauritius islands (Réunion hotspot), and Kaua'i (Hawaiian hotspot) largely based on the extensive sets of published radiometric ages. For example, Réunion is one of the best-dated volcanic islands in the world, with >500 absolute ages over 2500 km^2 that are supported by field observation of unconformities reflecting volcanic quiescence phases (Famin et al., 2022). All islands have high-resolution topographic data, which, along with radiometric ages, are crucial to reconstruct their pre-erosion topography and to constrain the timing when erosion started, which also provides a robust method for calculating erosion rates. In addition, Gayer et al. (2019) provided erosion rates of seven catchments of Réunion. Using these existing datasets, we calculate pre-erosion topography, determine basin average erosion rates, and empirically calibrate a simple bedrock river incision model (i.e. detachment-limited stream power model, see below) on all three islands and compare results to precipitation and climate data to explore climate role in shaping volcanic island landscapes.

2. Geological, climatic and geomorphological settings

2.1. Réunion Island

Réunion is the youngest island related to the Réunion hotspot, which is responsible for a volcanic chain that extends from the Deccan traps to Mauritius and Réunion islands. Réunion's edifice is composed of two volcanoes (Fig. 1a): the dormant Piton des Neiges (PdN, culminating at 3071 m), and active Piton de la Fournaise (PdF, 2632 m). The chronostratigraphy of PdN has been extensively studied (e.g. McDougall, 1971; Gillot and Nativel, 1982; Gillot et al., 1994; Kluska et al., 1997; Famin et al., 2022). Here, we adopt the latest chronostratigraphic review of Salvany et al. (2012), dividing the construction of PdN into five periods: La Montagne (2200 – 1800 ka), PN1 (1400 – 950 ka), PN2 (600 – 430 ka), PN3 (340 – 180 ka) and PN4 (140 – 27 ka). All the periods are separated by quiescence intervals during which erosion prevailed over construction. The history of the emerged part of PdF is subdivided into three periods: PF1 (560 – 290 ka), PF2 (250 – 65 ka) and PF3 (40 – 0 ka) (Bachèlery, 1981; Gillot and Nativel, 1989; Gillot et al., 1994; Merle et al., 2010; Michon et al., 2016). These periods are separated by erosion intervals, caldera events, and large-scale landslides (Merle et al., 2010).

Western PdN slopes are incised by narrow, elongated canyons, whereas northern PdN basins are deeper and larger (Fig. 1a). The island's central part is dominated by "cirques", which are amphitheater-shaped topographic depressions surrounding the PdN summit. The Marsouin paleo-cirque was carved into eastern PdN and then refilled by PN4 lavas, as was the Makes paleo-cirque (Fig. 1a). The western slopes of PdF have narrow and elongated canyons, whereas the central and eastern parts of this volcano display three large valleys: the Remparts, Langevin, and Est valleys (Fig. 1a). The Remparts and Langevin present-day valleys corresponds to a single palaeovalley that was refilled twice by lavas overflowing the Remparts and Morne Langevin caldera (Michon et al., 2016). The absence of lithospheric flexure (Lénat et al., 2009), sea level marker lithologies of various ages such as hyaloclastites, fossil beaches, and coral reefs, all at about present-day sea level (e.g. Montaggioni and Marin-Martin, 2020) point to the absence of subsidence or any significant vertical motion for the past 2000 kyr.

Réunion has a tropical climate characterized by a sharp contrast between the dry and rainy seasons and the occurrence of tropical cyclones. Trade winds blow from the southeast, which, combined with the island's relief above the atmospheric inversion layer, leads to one of the greatest rainfall gradients on Earth and produces an asymmetric precipitation pattern (Fig. 1a). Mean annual precipitation (MAP) rates range from 500 mm/yr to 2000 mm/yr for the leeward side of the island and from 2000 to 12,000 mm/yr for the windward side (Météo France). The volcanoes' high elevation, combined with the disappearance of atmospheric inversion layer in cyclonic conditions, are responsible for the cyclonic precipitation being centered around the island summit, i.e. farther west than the background annual precipitation (Réchou et al., 2019). Although the absolute rainfall values may have changed during the last 70 kyr, the spatial pattern of cyclonic and mean annual precipitation has not (Gayer et al., 2019). Global simulations based on Valdes et al. (2017) and Armstrong et al. (2023) show that the regional climate has remained stable for the past 800 ka (Steinig, pers. comm.) (**supplementary material S1**).

2.2. Mauritius Island

Mauritius is the second youngest island of the Réunion hotspot. The chronostratigraphy of Mauritius is subdivided into three volcanic series, separated by intervals of volcanic quiescence and erosion (McDougall and Chamalaun, 1969; Baxter, 1972; Perroud, 1982; Moore et al., 2011; Quidelleur and Famin, 2024): an older series (8900 – 4700 ka) and two, intermediate (3400 – 1700 ka) and younger (1000 – 14 ka), series of volcanic rejuvenation.

Mauritius culminates at 828 m (Fig. 1b). It has a high-elevation central plateau surrounded by low-elevation plains in the north and peripherical massifs that correspond to the eroded older units (Baxter, 1970). The central plateau presents a sharp escarpment on the western side of the island, whereas it has a smooth transition from 800 m to sea level on the eastern side. The plateau is deeply incised on the southwestern side, with headward erosion propagating toward the interior (Fig. 1b). In contrast, incision is reduced on the eastern side of Mauritius because it is mostly covered by the youngest volcanic products. Bathymetry and gravimetry data indicate the existence of a flexure basin SW of the island (Lénat et al., 2009). However, Montaggioni and Marin-Martin (2020) documented meager subsidence rates of Mauritius using fossil coral reefs for the last 400 kyr, ranging from 0.015 to 0.033 mm/yr. Much of the subsidence of Mauritius is, therefore, older than 400 ka.

Mauritius has a tropical climate similar to Réunion, with precipitation coming from the southeast. MAP rates range from ~600 to ~3950

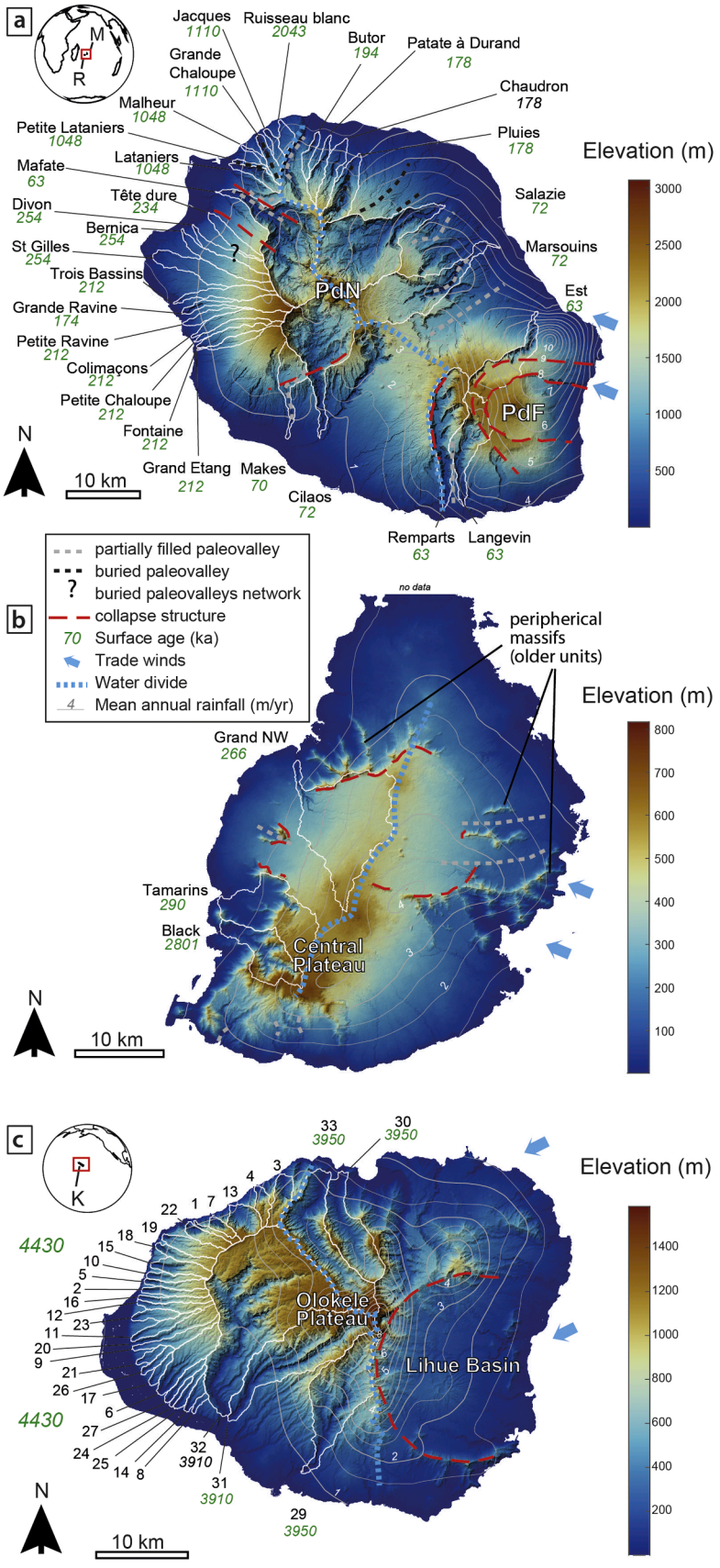

(caption on next page)

Fig. 1. a) Location of Réunion (R) and Mauritius (M) islands, Indian Ocean (Réunion hotspot) and topographic and climatic framework of Réunion Island. Color is a function of elevation and is superimposed on a shaded relief map based on 25-m-resolution data from Institut national de l'information géographique et forestière. Colormaps are from Crameri (2018). White lines delineate the drainage basins selected for this study. Grey lines are mean annual rainfall contours. PdN: Piton des Neiges; PdF: Piton de la Fournaise. b) Topographic and climatic framework of Mauritius Island based on 30-m-resolution SRTM data. c. Location of Kaua'i Island (K), Pacific Ocean (Hawai'i hotspot) and topographic and climatic framework of Kaua'i Island based on 30-m-resolution SRTM data. White lines delineate drainage basins analyzed by Ferrier et al. (2013b). Basins are numbered following Table 1 of Ferrier et al.'s (2013b) analysis. All western basins (3 to 14) correspond to 4430-ka-old surfaces.

mm/yr, and the maximum precipitation rates correspond to the plateau centre (Raja and Aydin, 2019). Given the low elevation of the Mauritius' summit, the entire island is likely to remain below the inversion layer all year long.

2.3. Kaua'i Island

Kaua'i, located on the Pacific plate, is related to the Hawai'i hotspot, which is responsible for the Hawaiian-Emperor chain. The chronostratigraphy of Kaua'i is divided into the shield (5140 – 3950 ka), post-shield (3950 – 3580 ka) and rejuvenated (3220 – 150 ka) series, the two latter being separated by a quiescence and erosion interval (McDonald et al., 1960; McDougall, 1964, 1979; Garcia et al., 2010, Sherrod et al., 2015).

Kaua'i Island's geomorphology (Fig. 1c**)** is characterized by the central Olokele plateau, bounded by the U-shaped Lihue basin in the east and steep relict surfaces of the shield volcano in the west, which are presently dissected by fluvial incision forming narrow canyons (Ferrier et al., 2013b). The Okolele plateau corresponds to a caldera that was refilled by lavas and is presently incised (McDonald et al., 1960). The Lihue basin was likely formed by structural collapse (Reiners et al., 1999). Subsidence of Kaua'i is evidenced by submerged marine terraces (Mark and Moore, 1987) and by bathymetry slope breaks around the island interpreted as paleoshorelines, which are located between 850 and 1000 m below sea level (Moore, 1987; Flinders et al., 2010).

Kaua'i experiences a precipitation range close to that of Réunion, from 500 mm/yr to 9500 mm/yr (PRISM Climate Group, 2006). Precipitation comes mostly from the northeast, due to the trade wind direction. Contrary to Réunion, the summit of Kaua'i, at 1593 m, is below the inversion layer. This results in the maximum rainfall rates (9500 mm/yr) being centered around the island summit and the lowest rainfall rates (500 mm/yr) being located on the western coast (Ferrier et al., 2013b), and the rainfall variability being lower than in Réunion (Gayer et al., 2019).

3. Material and methods

3.1. Topography and precipitation

Our study is based on digital elevation models (DEMs) that have the following horizontal resolution: 25 m and 5 m for Réunion (Institut national de l'information géographique et forestière), 30 m for Mauritius (SRTM), and 30 m and 10 m for Kaua'i (SRTM and U.S. Geological Survey). We performed paleotopography reconstructions using the highest-resolution DEMs and then resampled the results to the lowest resolution. We used the MAP 25-m-resolution grid compiled by Gayer et al. (2019) that covers the period 1981–2010 in Réunion, and the mean annual cyclonic precipitation (MACP) data from Gayer et al. (2019) that corresponds to eleven cyclones for the same period. For Mauritius, we used the isohyetal map for the period 1971–2000 from Anon., Mauritius Meteorological Services; for Kaua'i, the 30-m-resolution MAP data for the period 1971–2000 from the PRISM Climate Group (2006). These data have a high resolution but come from different sources; in order to ensure consistency between all study sites, we compare our data to a 1-km-resolution mean annual rainfall global dataset (Karger et al., 2021) in the **supplementary material S1.**

3.2. Drainage basin selection, paleotopography reconstructions, and erosion rate calculation

To perform quantitative topographic analysis, we used TopoToolbox v2 (Schwanghart and Scherler, 2014) and functions modified from Gallen and Wegmann (2017) and Gallen and Fernández-Blanco (2021). We selected basins whose area is greater than 1 km^2 (Fig. 1). A detailed justification for our selection of basins is provided in the **supplementary material S2**. We defined the initial topography of a given catchment as its surface immediately after the most recent eruption and before subsequent fluvial incision took place. For each basin, we interpolated uneroded remnants and topographic crests, or remnants of volcanic surfaces that refilled a pre-existing valley (**supplementary material S2)**. For the Mafate, Cilaos, Salazie, Remparts, Langevin, and Est basins, we used the paleoedifice reconstructions of Gayer et al. (2019). For Mauritius, we interpolated the remaining portions of the linear western escarpment of the plateau (Fig. 1b). We calculated the time-averaged erosion rate (E) of basins of Mauritius and Réunion islands by dividing the difference between the pre-incision and modern basin surfaces by the lava age of the incised surface and by the drainage area. We also ensured that our topographic reconstructions for Kaua'i were similar to those of Ferrier et al. (2013b) by also calculating erosion rates (**supplementary material S2**).

3.3. Numerical modelling of river incision

To go further than observations of erosion rates, and to understand the incision processes underlying the evolution of the river channels, we use a simple numerical model of river incision, the detachment-limited stream power model, that is widely used in geomorphology. We assume that hillslopes are locally coupled to channels such that incision rates provide an adequate proxy for erosion rates, which is based on studies that demonstrate hillslopes respond quickly to river channel base level fall (e.g., Gallen et al., 2011; Hurst et al., 2012). The detachment-limited stream power model is a convenient way to approximate long-term bedrock river incision (Howard and Kerby, 1983; Howard et al., 1994). This semi-empirical model links the long-term vertical incision rate (I) of a river through bedrock to the excess shear stress imposed by the water discharge on the riverbed:

$$I = k_e(\tau_s - \tau_c)^a \qquad \text{if } \tau_s > \tau_c \tag{1}$$

where, τ_c is the critical shear stress above which incision occurs, τ_s is the basal shear stress, and k_e is an erodibility constant. Assuming that τ_c is negligible, one can approximate τ_s, assuming A scales with discharge and the local channel slope represents the water surface slope. From this, the incision rate at a point in the river channel can be approximated as follows:

$$I(x) = K(P(x)A(x))^m S(x)^n \tag{2}$$

x is the horizontal distance to the river outlet. A and P are the drainage area and precipitation upstream from x; they represent a proxy for discharge. S is the local channel slope. K encapsulates bedrock lithology and soil properties, river discharge, vegetation cover (Jefferson et al., 2014) and chemical weathering (Murphy et al., 2016). m and n are positive constants that mean to describe channel hydraulic scaling and discharge scaling with changes in drainage area, as well as different incision processes, among other phenomena (Whipple, 2004). From Eq.

Table 1
Parameters used in the inverse model.

symbol	parameter	unit	parameter type	tested range of values
	initial and final river profiles		known	
t_{in}	initial time = volcanic surface age	yr	known	
m	area exponent		free	0.1–10
n	slope exponent		free	0.1–10
K	erodibility	m^{1-2m}/yr	free	10^{-40}–10^{-2}
A	upstream drainage area	m^2	calculated	
P	upstream annual precipitation	m/yr	calculated	
S	local channel slope		calculated	
I	incision rate	m/yr	calculated	

(2), the evolution of the elevation of the river channel through time can be described in a continuity equation:

$$\frac{\partial z}{\partial t} = U(x,t) - K(P(x)A(x))^m S(x)^n \quad (3)$$

where, U is the vertical motion and z is the elevation of the river channel.

The stream power model can be related to parameters in Flint's law that empirically describes the morphology of river longitudinal profiles (Flint, 1974):

$$S = k_s A^{-\theta} \quad (4)$$

where k_s is the channel steepness index, and θ is the concavity index (note that A can also be the precipitation-weighted to make is comparable to Eqs. (2) and 3). From Eq. (4), log-transformed plots of A vs S can be used to directly determine θ, which corresponds to the slope, and k_s, which is the y-intercept (e.g. Wobus et al., 2006). Extracting these parameters can help understand relationships between erosion, rock uplift, rock type, and fluvial topography when interpreted in the context of the detachment-limited stream power model (e.g. Snyder et al., 2000; Stock and Montgomery, 1999; Kirby and Whipple, 2001, 2012; Lague, 2014). This is because Eq. (2) can be rearranged to solve for local channel slope to show that:

$$\theta = m/n \quad (5)$$

and

$$k_s = \left(\frac{I}{K}\right)^{\frac{1}{n}} \quad (6)$$

k_s describes the channel slope normalized for upstream drainage area and, as shown in Eq. (6), is inferred to reflect aspects of incision rate, erodibility, and incision processes.

We followed the Bayesian approach of Gallen and Fernández-Blanco (2021) that uses a Markov chain Monte Carlo (MCMC) routine, which we describe in detail in the **supplementary material S3**, to invert topography for the stream power parameters. We obtain the erodibility K, the drainage area exponent m, and the slope exponent n (Table 1, Fig. 2, **supplementary material S3-S4**). For each basin, we constrained the model by setting the total incision duration as the volcanic surface age and using the present-day and reconstructed topographies. The MCMC routine works as follows: a random (n, m, K) suit is sampled within the tested ranges (Table 1) and input into the stream power model to simulate incision following Eq. (3). The resulting river profile is then compared to the present-day river profile. Each iteration can be either retained, or discarded based on the fit between modelled and observed data and the transition probability to a new state in the parameter space. This process is repeated 50,000 times and the parameters are defined based on the MCMC sample history after the chain has converged within a low misfit zone (i.e. solution). The procedure is performed twice: the first one uses a broad range of possible parameter values that allow us to narrow the range of tested parameter values, and the second uses on a smaller parameter range based on the results of the first one. The difference in DEM resolution between the islands, and our choice of timestep size, slightly influence our modelling results, but the impact is not significant (**supplementary material S3).**

In our model, we first assume that river incision begins immediately after an eruption ends. The occurrence of river channels in <600-yr-old lava flows of PdF (Albert et al., 2020) demonstrates that incision begins before the minimum timestep of our model, thus validating this assumption. Second, erodibility is assumed to be uniform through space and time in each individual basin. Although the erodibility of a lavas may change over time and between different flow lithologies, these differences are negligible compared to the case of orogenic settings where contrasting lithologies can lead to significant changes in erosion

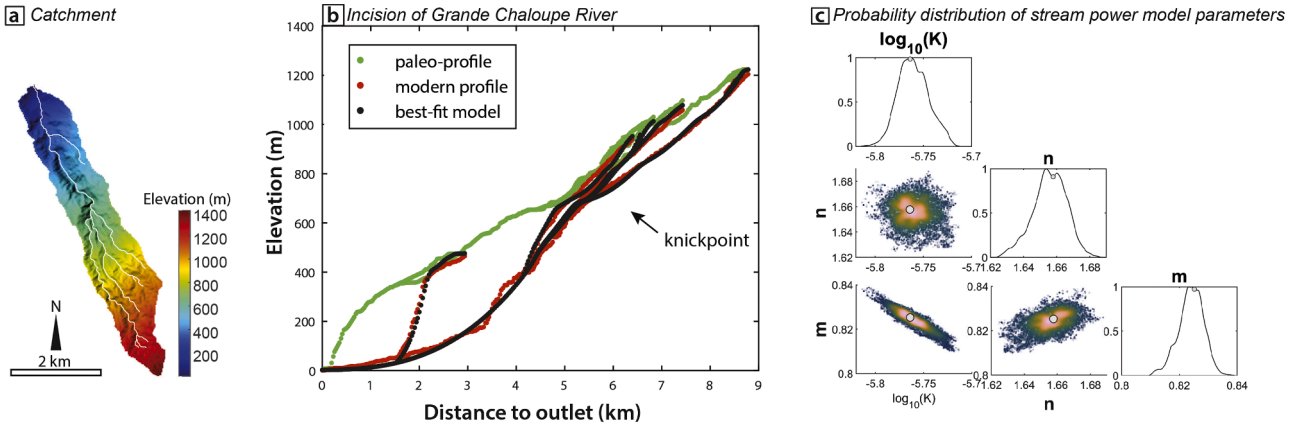

Fig. 2. Example of inverse and forward modelling of river incision of Grande Chaloupe River (Réunion Island). a) Catchment basin. b) Paleo-profile and observed modern river profile compared to the profile corresponding to the best-fit stream power law parameters ($n = 1.65$, $m = 0.83$, $K = 1 \times 10^{-5.76}$ m^{1-2m} yr^{-1}). c) Matrix plot of the posterior probability distributions of stream power model parameters from the Markov chain Monte Carlo inversion. The grey dot indicates the best-fit (maximum a posteriori) solution corresponding to the black profile on (b). Matrix plots of all basins are provided in the **supplementary material S4**.

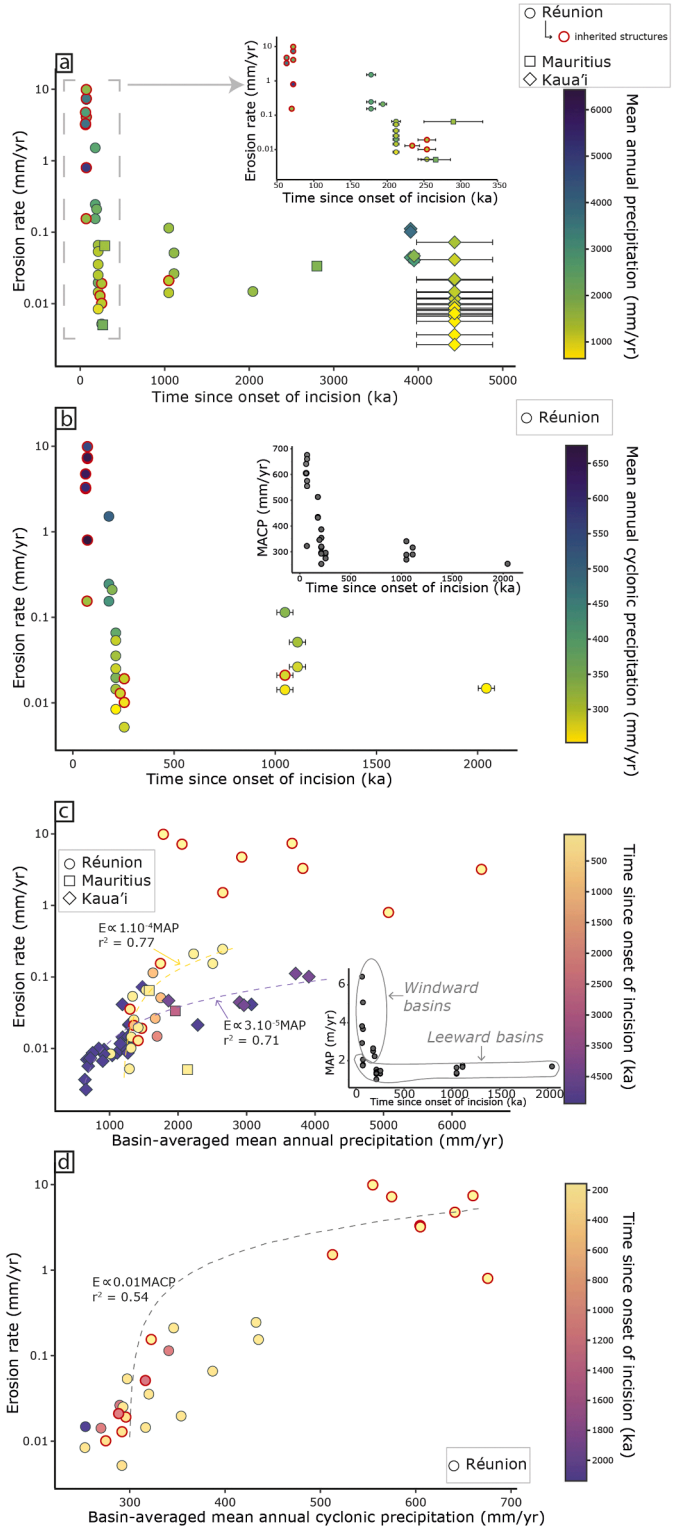

(caption on next column)

Fig. 3. Basin-averaged erosion rates plotted against time since incision started (a and b) and against basin-averaged climate variables (c and d). Dashed lines correspond to linear regressions discussed in the main text. a) Decimal logarithm of erosion rates of Réunion, Mauritius and Kaua'i plotted against paleosurface age with a close up of the 0 – 300 ka time range on (a). The color scale for (a) corresponds to mean annual basin-averaged precipitation rates and for (b) it corresponds to the mean annual cyclonic precipitation for Réunion Island. Error bars for erosion rates are smaller than the symbols and therefore not indicated. For Réunion Island, circles with a thick line indicate basins with a pre-existing structure. The inset in (b) shows the covariation of mean annual cyclonic precipitation rates (MACP) and volcanic surface ages of Réunion. The inset in (c) shows the covariation of mean annual precipitation rates (MAP) and volcanic surface ages of Réunion, with the dotted line indicating the water divide separating the leeward basins from the windward basins. Dotted lines in c) and d) correspond to the linear regressions between erosion rates and precipitation rates discussed in the main text. They are curved due to the logarithmic scale of the Y-axis. Erosion rates for Kaua'i are from Ferrier et al. (2013b).

efficiency (e.g. Gallen, 2018). Third, each basin drainage is assumed to be of fixed area over time. In Réunion, there is small amount of drainage area loss for some of the western basins because of cliff retreat of the cirques. Whipple et al. (2017) showed that water divide migration occurs at a slower rate than the river response time to a base level perturbation and that the effect of such perturbation is greater in small drainage basins. We apply the same reasoning here and assume that drainage area changes can be neglected in regard to incision for large basins (>1 km^2). We also explored the impact of the inversion results on a selected basin where we removed drainage area by shorting its upstream reaches (**Supplementary material S4**). The original and drainage-area modified results were comparable, suggesting that our assumption is reasonable (**Supplementary material S4**). The location of the volcanic centre of PdN has remained stable for the past 1400 kyr (Gayer et al., 2021). In Mauritius, the present-day water divide coincides with an N20°E-oriented rift zone of the older series (Perroud, 1982) and the young cones alignment, which is also parallel to the western escarpment of the plateau formed by the older series (Fig. 1b). Thus, the present-day water divide geometry of both islands was likely acquired early in their history. In Kaua'i, Ferrier et al. (2013a) suggested that the present-day drainage basin boundaries were established early in the volcano history because the relationship between drainage area and along-channel distance does not depend on volcanic surface ages (Seidl et al., 1994), which justifies our assumption of fixed drainage areas. Fourth, vertical motion is considered negligible over the duration of incision (U~0 in Eq. (3)), as do Ferrier et al. (2013a) for Kaua'i. The absence of subsidence since 2000 ka for Réunion, and very low subsidence rates since 400 ka for Mauritius, suggests that U~0 is a valid assumption for these two islands, except for Black River, which incises a 2800-ka-old surface on Mauritius. For Kaua'i, however, some subsidence does exist (Mark and Moore, 1987), i.e. incision might be overestimated in our models.

Because the n, m, and K, in the stream power model are codependent, a direct comparison between the erodibility values of all basins is not possible. Therefore, we performed a second set of inversions using $n = 1$ and a fixed concavity index (m/n ratio), to determine a normalized erodibility index K_n, that allows us to directly compare results from basin to basin and island to island, assuming a linear relationship between slope and incision rate. We chose a fixed concavity of 0.45, which is close to the median concavity index inferred from the first set of inversions (0.49) and also falls into the theoretical range of 0.35–0.6 predicted by Whipple and Tucker (1999). We used a similar inversion approach to the first inversions described above, but the only free variable was the normalized erodibility K_n.

Table 2
Precipitation variables and basin-averaged erosion rates of Réunion and western Mauritius islands inferred from paleotopographic reconstructions and eroded volumes.

	Basin name	*Pre-existing structure*	MAP	MACP	Eroded volume	Basin area	Basin median slope	stdev	Pre-incision median slope	stdev	Paleosurface age	±	Erosion rate	±	Reference
unit			mm/yr	mm/yr	m^3	m^2	°		°		kyr	kyr	mm/yr	mm/yr	
Reunion Island															
PN1															
	Ruisseau blanc		1693	253	1.2E+08	7.0E+06	17	10	11	5	2043	40	**1.5E-02**	8E-04	McDougall and Watkins (1973)
	Lataniers		1633	341	1.2E+09	9.8E+06	32	18	12	8	1048	40	**1.1E-01**	4E-03	McDougall (1971)
	Petite Lataniers	buried paleovalley	1353	288	5.9E+07	2.7E+06	20	11	11	5	1048	40	**2.1E-02**	8E-04	McDougall (1971)
	Grande Chaloupe	buried paleovalley	1746	316	4.9E+08	8.6E+06	27	15	12	7	1110	40	**5.1E-02**	2E-03	McDougall (1971)
	Jacques		1666	289	1.6E+08	5.5E+06	20	13	10	8	1110	40	**2.6E-02**	9E-04	McDougall (1971)
	Malheur		1307	270	3.5E+07	2.4E+06	18	9	12	5	1048	40	**1.4E-02**	5E-04	McDougall (1971)
PN3															
	Butor		2227	346	2.5E+08	6.2E+06	24	15	11	6	194	14	**2.1E-01**	3E-03	McDougall (1971)
	Pluies	paleovalley	2653	513	7.2E+09	2.7E+07	35	20	12	7	178	6	**1.5E+00**	5E-02	McDougall (1971); Gayer et al. (2019)
	Patate à Durand		2650	432	5.4E+08	1.2E+07	26	17	13	7	178	6	**2.4E-01**	8E-03	McDougall (1971)
	Chaudron		2505	435	4.8E+08	1.8E+07	19	17	13	9	178	6	**1.5E-01**	5E-03	McDougall (1971)
	St Gilles		1289	292	5.4E+07	4.1E+07	10	8	9	5	254	12	**5.2E-03**	2E-03	McDougall (1971)
	Fontaine		1335	297	1.4E+08	1.2E+07	15	11	13	6	212	4	**5.4E-02**	1E-03	Kluska (1997)
	Trois bassins		1316	317	5.2E+07	1.7E+07	13	9	11	5	212	4	**1.4E-02**	3E-04	Kluska (1997)
	Tête dure	buried paleovalley?	1416	292	3.7E+07	1.2E+07	15	11	13	6	234	10	**1.3E-02**	5E-04	Dumont et al. (2021); McDougall (1971)
	Bernica	buried paleovalley?	1313	275	5.5E+07	2.1E+07	12	10	10	6	254	12	**1.0E-02**	5E-04	Dumont et al. (2021); McDougall (1971)
	Colimaçons		1406	354	6.6E+07	1.6E+07	14	10	12	5	212	4	**2.0E-02**	4E-04	Kluska (1997)
	Divon	buried paleovalley?	1468	296	6.5E+07	1.3E+07	13	10	11	5	254	12	**1.9E-02**	9E-04	Dumont et al. (2021); McDougall (1971)
	Petite Chaloupe		1298	320	5.8E+07	7.7E+06	15	11	13	5	212	4	**3.5E-02**	7E-04	Kluska (1997)
	Grande Ravine		1531	387	2.6E+08	1.8E+07	12	12	11	5	174	16	**6.6E-02**	2E-03	Gillot and Nativel (1982)
	Petite Ravine		1014	253	2.9E+07	1.6E+07	13	9	12	5	212	4	**8.4E-03**	2E-04	Kluska (1997)
	Grand Etang		1353	293	4.2E+07	7.9E+06	15	11	13	5	212	4	**2.5E-02**	5E-04	Kluska (1997)
PN4															
	Marsouins*	paleovalley; paleocirque	5072	676		8.2E+07	17	19	5	13	72	3	**8.0E-01**	3E-01	Dumont et al. (2021); Gayer et al. (2019); Salvany et al. (2012);
	Salazie*	paleo-cirque	3664	660	6.5E+10	1.2E+08	29	20	12	11	72	3	**7.4E+00**	7E-01	Gayer et al. (2019); Salvany et al. (2012)
	Cilaos*	palaeo-cirque; collapse scar	1784	555	7.2E+10	1.0E+08	36	19	12	12	72	3	**9.9E+00**	5E-01	Gayer et al. (2019); Salvany et al. (2012)

(*continued on next page*)

Table 2 (*continued*)

unit	*Basin name*	*Pre-existing structure*	MAP	MACP	Eroded volume	Basin area	Basin median slope	stdev	Pre-incision median slope	stdev	Paleosurface age	±	Erosion rate	±	Reference
			mm/yr	mm/yr	m^3	m^2	°		°		kyr	kyr	mm/yr	mm/yr	
	Mafate*	collapse scar, paleovalley, paleo-cirque	2057	575	5.6E+10	8.9E+07	39	19	12	12	72	3	**7.2E+00**	7E-01	Gayer et al. (2019); Salvany et al. (2012); Kluska (1997); Gillot et al. (1994)
	Makes	paleovalley	1742	323	2.5E+08	2.3E+07	18	15	13	12	70	6	**1.5E-01**	6E-03	Salvany (2009)
Piton de la Fournaise	**Est***	collapse scar	6430	605	8.1E+09	3.9E+07	14	21	10	13	63	3	**3.2E+00**	7E-01	Gayer et al. (2019); Mairine and Bachèlery (1997); Gillot et al. (1994)
	Remparts*	collapse scar, Remparts paleovalley	2930	641	1.7E+10	5.8E+07	36	22	7	9	63	3	**4.8E+00**	1E+00	Gayer et al. (2019); Merle et al. (2010); Gillot and Nativel (1989)
	Langevin*	Remparts paleovalley	3821	605	8.3E+09	4.1E+07	20	21	8	9	63	3	**3.3E+00**	7E-01	Gayer et al. (2019); Merle et al. (2010); Gillot and Nativel (1989)
Mauritius Island	**Black**	plateau escarpment	1959		3.6E+09	3.8E+07	17	12	3	5	2801	30	**3.4E-02**	4E-04	McDougall and Chamalaun (1969)
	Tamarins	plateau escarpment	1579		1.2E+09	6.6E+07	4	10	2	6	290	40	**6.5E-02**	8E-03	Moore et al. (2011)
	Grand NW		2138		1.6E+08	1.2E+08	3	6	2	4	266	20	**5.1E-03**	4E-04	McDougall and Chamalaun (1969)

* Erosion rates from Gayer et al. (2019).

4. Results

Erosion rates cover five orders of magnitude in Réunion ($\sim10^{-3}$ to ~10 mm/yr, Fig. 3, Table 2). For Kaua'i, E covers only three orders of magnitude ($\sim10^{-3}$ to $\sim10^{-1}$ mm/yr) (**supplementary Table ST1; supplementary material S2**) that are similar to that of Ferrier et al. (2013b). For Mauritius, erosion rates range from $\sim10^{-3}$ to $\sim10^{-2}$ mm/yr. Comparing erosion rates of the three islands shows that there is a general decline in E with the time since the onset of incision, which we consider as represented by the age of the paleotopographic surface, from 63 ka to about 300 ka (Fig. 3a**- inset**) and no variation of E with time from 300 ka to 4000 ka. Réunion shows no apparent correlation between E and MAP when considering the entire dataset. However, when considering only low to moderate erosion rates of Réunion (<1 mm/yr), a positive trend appears between with MAP ($E \propto 1 \times 10^{-4}$ MAP, $N = 21$, $r^2 = 0.77$; Fig. 3c). When adding Mauritius to the dataset, r^2 equals 0.57.

The first MCMC inversion method, where n, m, and K are free parameters, converged toward a solution for 54 out of 64 catchment basins of all three islands. We excluded the ten remaining basins from our analysis (which we discuss in the **supplementary material S3)**. Both Réunion and Kaua'i islands exhibit a high dispersion in the best-fit slope exponent values (n) (Table 3, Fig. 4). Considering all three islands, n ranges from ~0.5 to ~6.2 and area exponent values (m) range from ~0.2 to ~2.9. Concavity values range from 0.2 to 1.5, with an average of 0.55 and a median of 0.49, which is close to the values of 0.45 to 0.5 reported in the literature (Harel et al., 2016; Kirby and Whipple, 2012). Results from Kaua'i exhibit generally lower values of n (0.4 to 2.6) than Réunion (0.76 to 6) and Mauritius (1.3 to 3.2). n values plotted against MACP rates in Réunion show an apparent positive trend, with $n \propto 0.07\text{MACP}$ ($N = 29$, $r^2 = 0.52$, p-value $< 10^{-14}$) (Fig. 4d**)**.

K_n, which we calculated forcing all basins to have the same n and m, covers four orders of magnitude and ranges from 2.3×10^{-7} to 9.8×10^{-4} $m^{0.1}$/yr (Fig. 5, Table 3). K_n is also lower in Kaua'i than in Réunion and Mauritius. For Réunion, no strong trend emerges between MAP and K_n when considering all basins; when considering only basins with low to moderate K_n values, there is a positive trend ($K_n \propto 4 \times 10^{-8}$ MAP, $N = 21$, $r^2 = 0.67$; Fig. 5a-c). There is a global positive trend between K_n and MACP rates on Réunion ($K_n \propto 2 \times 10^{-6}$ MACP, $N = 21$, $r^2 = 0.56$; Fig. 5b-d).

5. Discussion

5.1. Comparison of stream power calibration with previous studies

Our results suggest n values range between ~0.5 – 6, which is consistent with other empirical calibrations of the stream power model (Royden and Perron, 2013; Lague et al., 2014; Harel et al., 2016; Gallen and Wegmann, 2017; Gallen and Fernández-Blanco, 2021). Low n values found in our analysis of Kaua'i are consistent with the best-fit mean n value of 0.33 ± 0.02 reported by Ferrier et al. (2013a). Gayer et al. (2008) provide a slope exponent value of ~2 for basin 32, when it is 0.84 in this study; however, both values are not comparable, as the Gayer et al. (2008) model the lowering of the entire catchment's topography.

For basins 17 and 25 of Kaua'i (Table 3), our best-fit m values of 0.25 and 0.2 are consistent with the m values estimated by Stock and Montgomery (1999) for the same basins, ranging from 0.1 to 0.2. K_n indices are also consistent with Stock and Montgomery (1999) who calculated K values of $\sim10^{-6}$ m^{1-2m}/yr in catchments 17, 24, 25, and 27; however, Stock and Montgomery (1999) emphasize that slope exponent values are poorly constrained for these basins. Stock and Montgomery (1999) used a bedrock age of 5100 ka, whereas we used a bedrock age of 4430 ka based on more recent radiometric dating. We, therefore, infer that our approach for determining stream power parameters is generally consistent with aspects of previous studies.

Ferrier et al. (2013a) found that rock erodibility inferred from inverting topography using the stream power model, assuming a slope

Table 3
Model results.

	Basin name	m*	Solution range		n*	Solution range		$\log_{10}$K*	Solution range		**Normalized K**** m^{1-2m}/yr	solution range	
Reunion Island													
Piton des Neiges													
PN1													
	Ruisseau blanc	**0.40**	0.39	0.42	**0.76**	0.69	0.86	−5.32	−5.40	−5.25	**4.6E-06**	4.5E-06	4.7E-06
	Lataniers	**1.51**	1.50	1.52	**2.65**	2.62	2.67	−11.45	−11.53	−11.48	**2.2E-06**	2.2E-06	2.2E-06
	Petite Lataniers	**0.37**	0.34	0.40	**1.44**	1.34	1.62	−4.39	−4.50	−4.25	**1.0E-05**	1.0E-05	1.1E-05
	Grande Chaloupe	**0.83**	0.81	0.84	**1.66**	1.63	1.69	−5.76	−5.80	−5.72	**1.9E-05**	1.9E-05	1.9E-05
	Jacques	**0.52**	0.49	0.53	**1.56**	1.53	1.61	−4.82	−4.88	−4.68	**1.4E-05**	1.3E-05	1.4E-05
	Malheur	**0.42**	0.38	0.47	**0.88**	0.73	1.13	−5.06	−5.27	−4.85	**8.4E-06**	7.9E-06	9.0E-06
PN3													
	Butor	**1.02**	0.99	1.04	**2.48**	2.45	2.60	−5.47	−5.53	−5.30	**6.40E-05**	6.3E-05	6.5E-05
	Pluies	**2.35**	2.34	2.40	**4.18**	4.17	4.26	−9.40	−9.56	−9.39	**2.6E-04**	2.6E-04	2.6E-04
	Durand	**1.49**	1.47	1.51	**2.56**	2.52	2.59	−7.47	−7.55	−7.38	**7.5E-05**	7.4E-05	7.5E-05
	Chaudron	**0.86**	0.85	0.87	**1.59**	1.57	1.61	−5.60	−5.63	−5.56	**5.7E-05**	5.7E-05	5.8E-05
	St Gilles	**1.16**	1.10	1.20	**1.68**	1.55	1.80	−7.27	−7.45	−7.03	**1.1E-05**	1.0E-05	1.1E-05
	Fontaine	**0.70**	0.67	0.72	**3.12**	2.98	3.27	−4.25	−4.10	−4.11	**2.1E-05**	2.0E-05	2.2E-05
	Trois bassins	**0.83**	0.71	0.88	**0.55**	0.50	0.58	−6.64	−6.34	−6.95	**1.9E-05**	1.8E-05	2.0E-05
	Tête dure	**0.78**	0.68	0.80	**1.00**	0.95	1.10	−6.21	−6.25	−5.73	**1.1E-05**	1.1E-05	1.2E-05
	Bernica	**0.68**	0.65	0.71	**0.94**	0.90	0.98	−5.95	−5.82	−6.09	**1.1E-05**	1.1E-05	1.2E-05
	Colimaçons										**1.2E-05**	1.1E-05	1.2E-05
	Divon	**0.71**	0.67	0.75	**1.83**	1.76	1.90	−5.36	−5.52	−5.16	**1.3E-05**	1.0E-05	1.4E-05
	Petite Chaloupe	**0.63**	0.59	0.68	**1.25**	1.12	1.33	−5.25	−5.48	−5.06	**1.9E-05**	1.9E-05	2.0E-05
	Grande Ravine	**1.15**	1.12	1.17	**4.10**	4.00	4.10	−5.24	−5.33	−5.12	**2.5E-05**	2.5E-05	2.5E-05
	Petite Ravine	**0.55**	0.50	0.61	**1.09**	0.90	1.30	−5.15	−5.40	−4.90	**1.4E-05**	1.3E-05	1.5E-05
	Grand Etang	**0.32**	0.30	0.36	**1.33**	1.20	1.45	−4.17	−4.30	−4.02	**1.5E-05**	1.4E-05	1.6E-05
PN4													
	Marsouins	**1.08**	1.07	1.08	**1.89**	1.88	1.90	−6.07	−6.09	−6.06	**1.8E-04**	1.8E-04	1.8E-04
	Salazie	**2.91**	2.91	2.92	**6.20**	6.18	6.21	−9.52	−9.53	−9.49	**9.3E-04**	9.3E-04	9.3E-04
	Cilaos	**0.91**	0.91	0.92	**2.51**	2.50	2.52	−3.77	−3.78	−3.76	**1.2E-03**	1.2E-03	1.2E-03
	Mafate	**2.17**	2.16	2.17	**4.97**	4.95	4.99	−7.31	−7.34	−7.29	**9.8E-04**	9.8E-04	9.8E-04
	Makes	**0.84**	0.81	0.89	**0.79**	0.72	0.83	−5.90	−6.11	−5.88	**6.3E-05**	6.1E-05	6.4E-05
Piton de la Fournaise													
	Est	**1.43**	1.42	1.44	**3.12**	3.10	3.13	−7.10	−7.12	−7.06	**2.4E-04**	2.4E-04	2.5E-04
	Remparts	**2.47**	2.46	2.48	**4.34**	4.32	4.36	−9.89	−9.93	−9.85	**7.0E-04**	7.0E-04	7.0E-04
	Langevin	**1.11**	1.11	11.12	**2.92**	2.91	2.93	−4.90	−4.91	−4.89	**4.1E-04**	4.1E-04	4.1E-04
Mauritius Island													
	Black	**1.18**	1.12	1.23	**3.19**	3.06	3.28	−5.36	−5.54	−5.18	**2.0E-05**	1.95E-05	1.97E-05
	Tamarins	**0.22**	0.20	0.29	**1.28**	1.25	1.31	−2.82	−3.19	−2.72	**6.8E-05**	6.73E-05	6.88E-05
	Grand NW	**0.79**	0.73	0.81	**2.25**	0.73	0.81	−4.62	−4.72	−4.30	**2.7E-05**	2.5E-03	7.50E-03
Kauai'i Island													
Awa'awapuhi	**1**	**0.77**	0.67	0.83	**0.52**	0.50	0.57	−6.75	−6.96	−6.37	**3.8E-06**	3.76E-06	3.90E-06
Haeleele	**2**										**5.8E-06**	5.73E-06	5.86E-06
Hanakapi'ai	**3**	**0.21**	0.21	0.22	**0.87**	0.86	0.87	−4.31	−4.34	−4.30	**5.9E-06**	5.92E-06	5.97E-06
Hanakoa	**4**										**2.7E-06**	2.64E-06	2.72E-06
Hikimoe	**5**	**0.54**	0.50	0.58	**1.14**	1.09	1.17	−5.56	−5.77	−5.42	**4.9E-06**	4.80E-06	4.99E-06
Hoea	**6**	**0.40**	0.39	0.41	**0.79**	0.78	0.83	−5.08	−5.11	−5.02	**8.9E-06**	8.84E-06	8.95E-06
Honopu	**7**	**0.46**	0.45	0.47	**1.57**	1.55	1.58	−5.02	−5.06	−4.99	**8.8E-06**	8.75E-06	8.83E-06
Huluhulunui	**8**										**5.7E-06**	5.11E-06	7.91E-06
Kaawaloa	**9**										**7.5E-06**	7.41E-06	7.59E-06
Kaaweiki	**10**	**0.59**	0.57	0.62	**0.59**	0.54	0.62	−5.94	−6.08	−5.88	**6.6E-06**	6.46E-06	6.67E-06
Kahelunui	**11**	**0.47**	0.44	0.50	**0.50**	0.45	0.55	−5.76	−5.84	−5.63	**5.8E-06**	5.74E-06	5.93E-06
Kahoaloha	**12**	**0.66**	0.61	0.66	**0.62**	0.58	0.67	−6.44	−6.61	−6.25	**4.1E-06**	4.02E-06	4.21E-06
Kalalau	**13**	**0.57**	0.55	0.61	**2.36**	2.46	2.53	−5.02	−5.09	−4.97	**1.1E-05**	1.14E-05	1.15E-05
Kapilimao	**14**										**8.4E-06**	8.22E-06	8.61E-06
Kauhao	**15**	**0.50**	0.50	0.51	**0.75**	0.74	0.75	−5.39	−5.40	−5.37	**1.1E-05**	1.05E-05	1.06E-05
Ka'ula'ula	**16**	**0.35**	0.32	0.39	**0.64**	0.61	0.67	−5.22	−5.36	−5.12	**5.0E-06**	4.90E-06	5.05E-06
Kuapa'a[SM]	**17**	**0.25**	0.21	0.30	**0.52**	0.42	0.59	−5.00	−5.14	−4.83	**5.9E-06**	5.68E-06	6.19E-06
Makaha	**18**	**0.41**	0.40	0.42	**0.86**	0.86	0.87	−5.13	−5.18	−5.10	**6.2E-06**	6.19E-06	6.27E-06
Miloli'i	**19**	**0.33**	0.32	0.35	**0.62**	0.61	0.64	−5.22	−5.28	−5.17	**3.2E-06**	3.13E-06	3.22E-06
Nahomalu	**20**										**2.3E-07**	2.28E-07	2.39E-07
Niu	**21**	**0.35**	0.29	0.39	**0.41**	0.37	0.51	−5.38	−5.54	−5.14	**6.2E-06**	5.91E-06	6.44E-06
Nu'alolo	**22**	**0.65**	0.63	0.67	**1.62**	1.59	1.65	−5.83	−5.88	−5.75	**5.4E-06**	5.38E-06	5.46E-06
'Ohai'ula	**23**	**0.46**	0.43	0.50	**0.76**	0.68	0.79	−5.58	−5.74	−5.46	**4.3E-06**	4.16E-06	4.43E-06
Paua[SM]	**24**										**5.2E-06**	4.74E-06	5.62E-06
Wai'aka[SM]	**25**	**0.21**	0.17	0.29	**0.47**	0.47	0.54	−4.89	−5.09	−4.75	**7.2E-06**	6.85E-06	7.52E-06
Wailao	**26**	**0.34**	0.29	0.37	**0.42**	0.33	0.48	−5.28	−5.44	−5.11	**7.2E-06**	6.94E-06	7.52E-06
Waipao[SM]	**27**										**6.9E-06**	6.66E-06	7.11E-06
Hanapepe	**29**	**0.95**	0.95	0.97	**2.61**	2.60	2.64	−5.46	−5.59	−5.42	**1.5E-05**	1.46E-05	1.46E-05
Lumahai	**30**										**1.5E-05**	1.52E-05	1.52E-05
Makaweli	**31**	**0.37**	0.37	0.39	**0.99**	0.99	1.00	−5.43	−5.53	−5.42	**1.1E-06**	1.09E-06	1.09E-06
Waimea	**32**	**0.40**	0.40		**0.84**	0.84	0.84	−4.70	−4.71	−4.70	**1.6E-05**	1.57E-05	1.57E-05
Wainiha	**33**	**0.34**	0.34	0.34	**0.59**	0.59	0.59	−4.59	−4.60	−4.59	**1.8E-05**	1.75E-05	1.76E-05

* Recovered from inversion.
** Assuming $m = 0.45$ and $n = 1$. SM: Stock and Montgomery (1999) determined that m ranges from 0.1 to 0.2 for these basins, using a bedrock age of 5.1 Myr.

exponent of one correlates with MAP in Kaua'i, which contradicts our results where K_n is does not change with MAP (Fig. 5c). However, differences in modelling approaches likely explain this discrepancy. Ferrier et al. (2013a) selected single channels with a low spatial precipitation variability. In contrast, this study focuses on entire drainage networks that likely experience a higher spatial rainfall variability. Additional modelling based on single main channels only yields normalized erodibility indices that are not significantly different from those presented here (**supplementary material S3**).

5.2. Erosion rates, topographic inheritance, and age of watersheds

We first explore the influence of volcanic features and volcanism timing on the rates and patterns of erosion, which could obscure the potential climate signals we aim to identify. A hypothesis to explain the five orders of magnitude of erosion rates is topographic inheritance. For example, a basin with a steeper paleosurface might experience a higher erosion rate during its early evolution than a basin with a lower initial slope. To test this hypothesis, we calculated the median slope of the reconstructed paleosurface for each basin of Réunion Island (Fig. 6a) and performed the same analysis for Kaua'i and Mauritius. Most median paleoslope values of Réunion and Kaua'i islands range between 5° and 13°, which corresponds to typical gentle slopes of shield volcanoes (Grosse and Kervyn, 2018). Low present-day and paleoslopes of Mauritius are due to the central plateau. Across all three islands, erosion rate values appear to increase slightly with median paleoslope values, but the relationship is not significant, and no relationship exists for a single island. Thus, the pre-incision slope of the basins is likely not directly linked to their erosion rates. The median slope of the present-day basins does not exhibit any obvious correlation with the age of the volcanic surface from 60 ka to 4000 ka (Fig. 6b), suggesting that slope is not strongly affected by the aging of the basins as they evolve from young to mature.

Alternatively, structural boundaries may play a role in increasing the range of erosion rates of the three islands. Indeed, discontinuities are known to guide river incision and enhance erosion (Hildenbrand et al., 2008). Given the polygenic history of construction and erosion of the three islands, many basins may have developed on inherited structures. However, in western Réunion, the Bernica, Tête Dure and Divon basins (Fig. 1a) are developed on buried paleovalley systems (Dumont et al., 2021), and yet their erosion rates are within the range as the other basins nearby with the same age and unrelated to any pre-existing structure. Importantly, these basins follow the same trends as other basins do with climate parameters that we discuss later, suggesting they do not behave in a distinct way. Thus, even if structural discontinuities may guide rapid river incision in special cases, there must be another factor at play to explain the general results.

The apparent decline in E with the time since the onset of incision from 63 ka to about 300 ka (Fig. 3a**- inset**) constitutes a potential limitation to our study that aims at isolating climate signals in the erosion record. Importantly, in the same time range, MAP and MACP rates also decrease with the paleosurfaces ages (Fig. 3b**– inset**; Fig. 3c**- inset**). This inverse correlation is due to the spatial distribution of the drainage basins of Réunion and the southeastern location of active PdF. For example, all basins older than 150 ka are confined in northern and western Réunion (Fig. 1a**)**. They are, therefore, exposed to low rainfall rates. Conversely, most young basins ($\leq$72 ka) are on the windward side of the island. Thus, it is plausible that both inverse correlations (between surface age and E, and between surface age and precipitation rates) are linked through climate, although we cannot eliminate the possibility of a timescale bias in our dataset. From 300 ka to 4000 ka, there is no clear trend between ages and erosion rates. A process that might link age and incision is subsidence, which elevates the local base level of volcanic islands and could lead to slower river incision, resulting in lower erosion. However, we observe a decrease in E from young to old catchments within Réunion, for which vertical motion has been negligible since its early phases (Lénat et al., 2009; Montaggioni and Marin-Martin, 2020). Subsidence is, therefore, not likely the cause for the observed decline in erosion rates with respect to the age of onset for incision.

5.3. Erosion rates, stream power law parameters, and climate variables

We compare erosion rates (Fig. 3), slope exponent values (Fig. 4), and normalized erodibility values (Fig. 5), to mean annual precipitation rates for all three islands, and to mean annual cyclonic precipitation rates for Réunion Island (similar data does not exist for the two other islands). Since rivers in Réunion are not in equilibrium, a climate signal (if any) can be recorded in erosion rates (e.g., Marder and Gallen, 2023). The presence of a correlation between E and MAP for low to moderate erosion rates, but not for the entire dataset, suggests that there might be two processes at play in Réunion: MAP controlling the pattern of low to moderate erosion rates, and another process controlling high erosion rates (>1 mm/yr), such as the daily precipitation variability proposed by Gayer et al. (2019) (Fig. 3c). Positive relationships between E and MAP are observed for Kaua'i, but the functional relationship is different than for the moderate erosion rate basins in Réunion (Fig. 3c). This suggests that MAP likely affects erosion rates on islands above both hotspots, but important differences exist that affect the scaling of the relationship. For Réunion, there is a positive relationship between E and MACP, which implies cyclonic storms might better predict E on the island than MAP and might help explain differences with Kaua'i (Fig. 4d). As pointed out by Gayer et al. (2019), Kaua'i and Réunion strikingly differ in shape: Réunion is 1.5 km higher in elevation than Kaua'i, where storm-induced precipitation likely coincides with the mean annual rainfall spatial distribution. This is perhaps why Réunion and Kaua'i have different sensitivities to mean annual rainfall, but more research is needed to understand this discrepancy. For the same hypothetical increase in MAP, erosion rates of Réunion would increase more than in Kauai, as shown by the trend lines in Fig. 3c.

The best-fit slope exponents, n, show no clear relationship with volcanic surface ages among all islands (Fig. 4a-b**)**. The relationship between n and MAP for all islands shows a generally positive but not significant trend (Fig. 4c). However, a positive trend between n and MACP for Réunion suggests that some climate parameters might affect geomorphic process and river incision (Fig. 4d), although our knowledge of past cyclonic precipitation pattern is limited. The fact that MAP in Kaua'i correlates strongly with E, but not with n, suggests that this parameter might be influenced by other factors, such as soil and vegetation cover (Ghestem et al., 2011; Murphy et al., 2016; Gayer et al., 2019).

Considering all three islands, 16 basins out of 54 yield n values greater than 2 (mostly Réunion and Mauritius) (Fig. 4**)**. In the detachment-limited stream power framework, this nonlinear relationship is predicted by models that include thresholds for the initiation of bedrock incision and the statistical distribution of floods that breach these thresholds (Tucker, 2004; Lague et al., 2005; Lague, 2014; Deal et al., 2018). The stochastic-threshold incision models (STIMs) indicate that when incision thresholds are significant, n values increase with decreasing variability of flood distributions. Empirical and theoretical studies show that flood variability typically declines as MAP increases (Molnar et al., 2006; Rossi et al., 2016; Deal et al., 2018). It is then possible that the changes in n with MAP and MACP can be explained by a STIM-type model. If correct, our results imply incision thresholds are important in Réunion, where n increases with MAP and MACP and are likely negligible in Kaua'i where no relationship exists (Fig. 4c,d). However, this is speculation as the data is scattered and more research should focus on incision thresholds and relationships between incision and hydroclimate in both regions.

Contrary to Réunion, where most n values are greater than one, most n values of Kaua'i are smaller than one. This is intriguing because it suggests fundamentally different relationships between erosion and

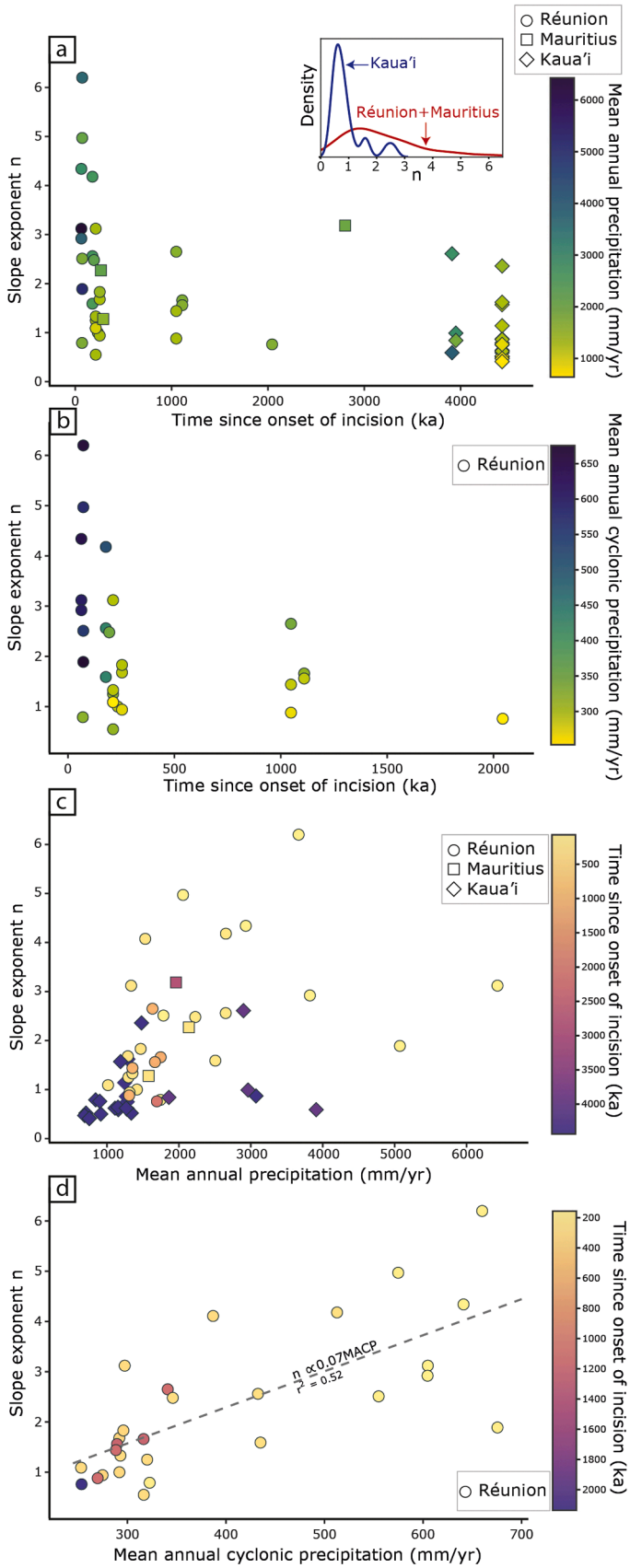

Fig. 4. Best-fit slope exponent values inferred from inverse modelling plotted against (a, b) time since onset of incision (volcanic paleosurface age), (c) basin-averaged mean annual precipitation for Réunion, Mauritius and Kaua'i islands and (d) basin-averaged mean annual cyclonic precipitation for Réunion Island. The inset in (a) shows the contrasting kernel density plots of n values of Kaua'i Island (blue curve) and Mauritius and Réunion (red). The dotted lines in c) and d) show the linear regression between discussed in the main text. They are curved due to the logarithmic scale of the Y-axis.

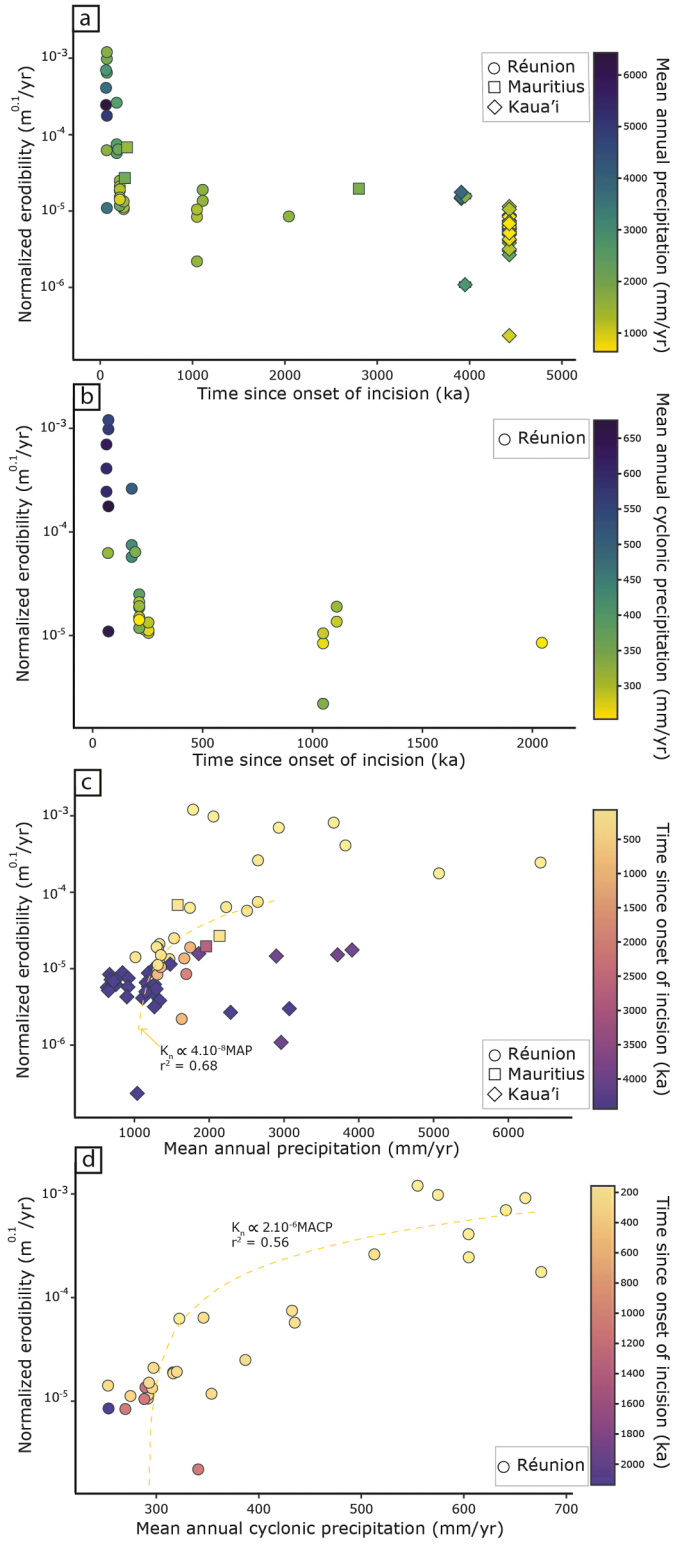

Fig. 5. a) Normalized erodibility K_n (logarithmic scale) recovered from the inversion assuming $m = 0.45$ and $n = 1$ plotted against the mean annual precipitation rates for all three islands (a) and against the cyclonic precipitation rates for Réunion Island (b). The color code refers to the volcanic paleosurface age as in Fig. 5c, d. The dotted lines in c) and d), which are curved due to the logarithmic scale of the Y-axis, correspond to the linear regressions between K_n and MAP, and between K_n and MACP.

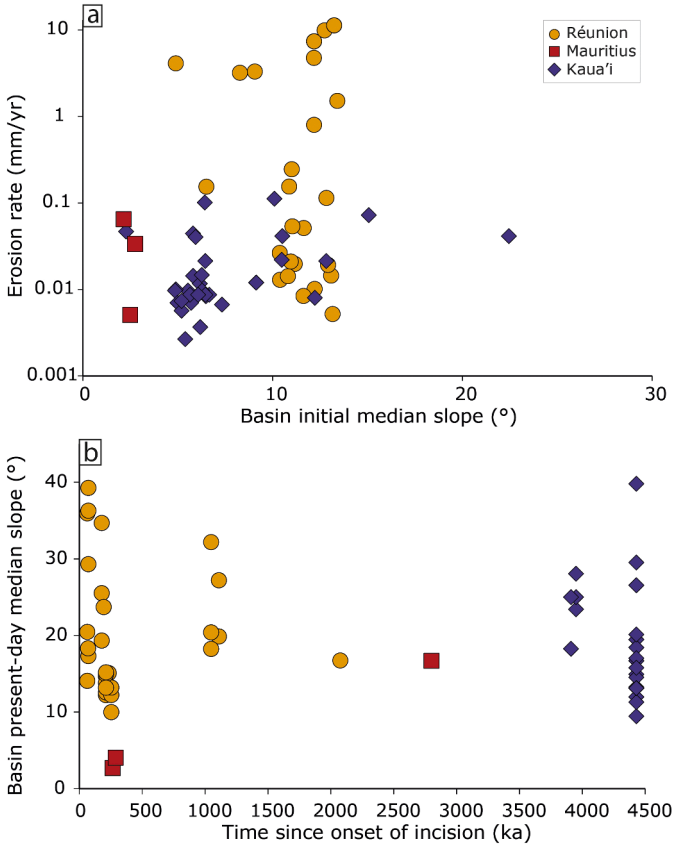

Fig. 6. a) Decimal logarithm of erosion rates of Réunion, Kaua'i and Mauritius islands plotted against the median slope of the basin paleosurface. Note that the slope standard deviation is extremely high but is not shown for more clarity. b) Present-day median basin slope plotted against paleosurface age.

channel steepness. For example, if $n = 0.5$, and considering a hypothetical incision rate increasing from 1 to 2 mm/yr, k_s would be multiplied by 4, producing a steeper fluvial relief; if $n = 1$, k_s would double; if $n = 6$, k_s would barely increase. Although rare, n values smaller than one have been reported in steep environments such as active normal faults with carbonate bedrock (Royden and Perron, 2013; Gallen and Wegmann, 2017), but the exact mechanism(s) responsible for $n < 1$ is unclear.

6. Conclusion

We document long-term erosion rates of three hotspot volcanic islands: Réunion (9.9 ± 0.5 mm/yr to $5.2 \times 10^{-3} \pm 2.3 \times 10^{-4}$ mm/yr), Mauritius ($6.5 \times 10^{-2} \pm 7.8 \times 10^{-3}$ to $5.1 \times 10^{-3} \pm 3.5 \times 10^{-4}$ mm/yr) and Kaua'i ($2.6 \times 10^{-3} \pm$ to 9.8×10^{-2} mm/yr), the latter being consistent with previous inferences. Our empirical calibration of the stream power incision model on all islands yields best-fit slope exponent values ranging from 0.5 to 6. We calculate a normalized erodibility coefficient K_n ranging from 2.3×10^{-7} to 9.8×10^{-4} m^{1-2m}/yr. Erosion rates and K_n on Réunion decrease with the age of the volcano during the first 300 kyr of its evolution, which is likely related to the covariation between climate variables and volcanism age. Cyclonic precipitation rates positively influence erosion rates and n values in Réunion. Erosion rates of both Kauai and Réunion (with Mauritius) are influenced by mean annual precipitation rates. Our study highlights major differences in stream power parameters, sensitivity of fluvial relief to incision, and sensitivity of incision to climate between Kaua'i and Réunion. Future research will involve i) quantifying the incision threshold on volcanic islands; ii) quantifying the morphological evolution over time of a

drainage basin since its birth; iii) investigating the cause for slope exponents values smaller than one.

CRediT authorship contribution statement

Loraine Gourbet: Writing – review & editing, Writing – original draft, Project administration, Methodology, Investigation, Formal analysis, Conceptualization. **Sean F. Gallen:** Writing – review & editing, Writing – original draft, Project administration, Methodology, Investigation, Formal analysis, Conceptualization. **Vincent Famin:** Writing – review & editing, Investigation, Formal analysis. **Laurent Michon:** Writing – review & editing. **Miangaly Olivia Ramanitra:** Investigation. **Eric Gayer:** Writing – review & editing, Methodology, Formal analysis.

Declaration of competing interest

The authors declare that they have no known competing financial interests or personal relationships that could have appeared to influence the work reported in this paper.

Data availability

The codes developed to conduct the data inversion can be cited and found at https://github.com/sfgallen/Gourbet_Volc_River_Inversions.

Acknowledgements

We wish to thank Dr. Sebastian Steinig for his expertise on climate evolution and for running global climate simulations, which greatly improved this manuscript; we also thank Dr. Paul Valdes for providing the climate model data. This research received funding from the programme TelluS of the Institut National des Sciences de l'Univers, CNRS, awarded to L. Gourbet and V. Famin. We thank Carolina Lithgow-Bertelloni and two anonymous reviewers for their help.

Supplementary materials

Supplementary material associated with this article can be found, in the online version, at doi:10.1016/j.epsl.2024.118973..

References

Adams, B.A., Whipple, K.X., Forte, A.M., Heimsath, A.M., Hodges, K.V., 2020. Climate controls on erosion in tectonically active landscapes. Sci. Adv. 6, eaaz3166. https://doi.org/10.1126/sciadv.aaz3166.

Albert, S., Flores, O., Michon, L., Strasberg, D., 2020. Dating young (<1000 yr) lava flow eruptions of Piton de la Fournaise volcano from size distribution of long-lived pioneer trees. J. Volcanol. Geotherm. Res. 401, 106974. https://doi.org/10.1016/j.jvolgeores.2020.106974.

Armstrong, E., Tallavaara, M., Hopcroft, P.O., Valdes, P., 2023. North African humid periods over the past 800,000 years. Nat. Commun. 14, 5549. https://doi.org/10.1038/s41467-023-41219-4.

Baxter, A.N., 1972. Magmatic Evolution of Mauritius, Western Indian Ocean. University of Edinburgh, Scotland. Ph.D. Thesis.

Crameri, F., 2018. Scientific Colour Maps. Zenodo. https://doi.org/10.5281/zenodo.1243862.

Deal, E., Braun, J., Botter, G., 2018. Understanding the role of rainfall and hydrology in determining fluvial erosion efficiency. J. Geophys. Res. Earth Surf. 123, 744–778. https://doi.org/10.1002/2017JF004393.

Dumont, M., Reninger, P.A., Aunay, B., Pryet, A., Jougnot, D., Join, J.L., Michon, L., Martelet, G., 2021. Hydrogeophysical characterization in a volcanic context from local to regional scales combining airborne electromagnetism and magnetism. Geophys. Res. Lett. 48. https://doi.org/10.1029/2020GL092000.

Famin, V., Paquez, C., Danišík, M., Gardiner, N.J., Michon, L., Kirkland, C.L., Berthod, C., Friedrichs, B., Schmitt, A.K., Monié, P., 2022. Multitechnique geochronology of intrusive and explosive activity on piton des neiges volcano, réunion island. Geochem. Geophys. Geosyst. 23. https://doi.org/10.1029/2021GC010214.

Ferrier, Ken L., Huppert, K.L., Perron, J.T., 2013a. Climatic control of bedrock river incision. Nature 496, 206–209. https://doi.org/10.1038/nature11982.

Ferrier, K.L., Perron, J.T., Mukhopadhyay, S., Rosener, M., Stock, J.D., Huppert, K.L., Slosberg, M., 2013b. Covariation of climate and long-term erosion rates across a steep rainfall gradient on the Hawaiian island of Kaua'i. Geol. Soc. Am. Bull. 125, 1146–1163. https://doi.org/10.1130/B30726.1.

Flinders, A.F., Ito, G., Garcia, M.O., 2010. Gravity anomalies of the Northern Hawaiian Islands: implications on the shield evolutions of Kauai and Niihau. J. Geophys. Res. 115, B08412. https://doi.org/10.1029/2009JB006877.

Gallen, S.F., Fernández-Blanco, D., 2021. A new data-driven bayesian inversion of fluvial topography clarifies the tectonic history of the corinth rift and reveals a channel steepness threshold. J. Geophys. Res. Earth Surf. 126. https://doi.org/10.1029/2020JF005651.

Gallen, S.F., Wegmann, K.W., 2017. River profile response to normal fault growth and linkage: an example from the Hellenic forearc of south-central Crete. Greece. Earth Surf. Dynam. 5 (1), 161–186. https://doi.org/10.5194/esurf-5-161-2017.

Gallen, S.F., Wegmann, K.W., Frankel, K.L., Hughes, S., Lewis, R.Q., Lyons, N., Paris, P., Ross, K., Bauer, J.B., Witt, 2011. Hillslope response to knickpoint migration in the Southern Appalachians: implications for the evolution of post-orogenic landscapes. Earth Surf. Proce. Landforms 36 (9), 1254–1267. https://doi.org/10.1002/esp.2150.

Gallen, S.F., 2018. Lithologic controls on landscape dynamics and aquatic species evolution in post-orogenic mountains. Earth Planet. Sci. Lett. 493, 150–160. https://doi.org/10.1016/j.epsl.2018.04.029.

Garcia, M.O., Swinnard, L., Weis, D., Greene, A.R., Tagami, T., Sano, H., Gandy, C.E., 2010. Petrology, geochemistry and geochronology of Kaua'i lavas over 4·5 Myr: implications for the origin of rejuvenated volcanism and the evolution of the hawaiian plume. J. Petrolo. 51, 1507–1540. https://doi.org/10.1093/petrology/egq027.

Gayer, E., Mukhopadhyay, S., Meade, B.J., 2008. Spatial variability of erosion rates inferred from the frequency distribution of cosmogenic ^{3}He in olivines from Hawaiian river sediments. Earth Planet. Sci. Lett. 266, 303–315. https://doi.org/10.1016/j.epsl.2007.11.019.

Gayer, E., Michon, L., Louvat, P., Gaillardet, J., 2019. Storm-induced precipitation variability control of long-term erosion. Earth Planet. Sci. Lett. 517, 61–70. https://doi.org/10.1016/j.epsl.2019.04.003.

Gayer, E., Michon, L., Villeneuve, N., 2021. Volcanic island multi-stage construction inferred from a simple geometrical approach: example of Réunion Island. Geomorphology 392, 107900. https://doi.org/10.1016/j.geomorph.2021.107900.

Ghestem, M., Sidle, R.C., Stokes, A., 2011. The influence of plant root systems on subsurface flow: implications for slope stability. Bioscience 61, 869–879. https://doi.org/10.1525/bio.2011.61.11.6.

Gillot, P.-Y., Nativel, P., 1982. K-Ar chronology of the ultimate activity of Piton des Neiges volcano, Réunion Island, Indian Ocean. J. Volcanol. Geotherm. Res. 13, 131–146. https://doi.org/10.1016/0377-0273(82)90024-5.

Gillot, P.Y., Nativel, P., 1989. Eruptive history of the Piton de la Fournaise volcano, Réunion island, Indian Ocean. J. Volcanol. Geotherm. Res. 36, 53–65.

Gillot, P., Lefevre, J., Nativel, P., 1994. Model for the structural evolution of the volcanoes of Réunion Island. Earth Planet. Sci. Lett. 122, 291–302.

Grosse, P., Kervyn, M., 2018. Morphometry of terrestrial shield volcanoes. Geomorphology 304, 1–14. https://doi.org/10.1016/0j.geomorph.2017.12.017.

Harel, M.-A., Mudd, S.M., Attal, M., 2016. Global analysis of the stream power law parameters based on worldwide ^{10}Be denudation rates. Geomorphology 268, 184–196. https://doi.org/10.1016/j.geomorph.2016.05.035.

Hildenbrand, A., Gillot, P.-Y., Marlin, C., 2008. Geomorphological study of long-term erosion on a tropical volcanic ocean island: tahiti-Nui (French Polynesia). Geomorphology 93, 460–481. https://doi.org/10.1016/j.geomorph.2007.03.012.

Hurst, M.D., Mudd, S.M., Walcott, R., Attal, M., Yoo, K., 2012. Using hilltop curvature to derive the spatial distribution of erosion rates. J. Geophys. Res Earth Surf. 117 (F2). https://doi.org/10.1029/2011JF002057.

Jefferson, A.J., Ferrier, K.L., Perron, J.T. and Ramalho, R., 2014. Controls on the hydrological and topographic evolution of shield volcanoes and volcanic ocean islands. In: The Galápagos: a Natural Laboratory For the Earth Sciences (eds K.S. Harpp, E. Mittelstaedt, N. d'Ozouville and D.W. Graham). https://doi.org/10.1002/9781118852538.ch10.

Karger, D.N., Wilson, A.M., Mahony, C., Zimmermann, N.E., Jetz, W., 2021. Global daily 1km land surface precipitation based on cloud cover-informed downscaling. Sci. Data. https://doi.org/10.1038/s41597-021-01084-6.

Kirby, E., Whipple, K., 2001. Quantifying differential rock-uplift rates via stream profile analysis. Geol 29, 415. https://doi.org/10.1130/0091-7613(2001)029<0415:QDRURV>2.0.CO;2.

Kirby, E., Whipple, K.X., 2012. Expression of active tectonics in erosional landscapes. J. Struct. Geol. 44, 54–75. https://doi.org/10.1016/j.jsg.2012.07.009.

Kluska, J.M., 1997. Evolution Magmatique Et Morpho-Structurale Du Piton des Neiges au Cours Des Derniers 500000 ans. Paris XI University, p. 125. Ph.D. Thesis.

Lénat, J.-F., Merle, O., Lespagnol, L., 2009. La Réunion: an example of channeled hot spot plume. J. Volcanol. Geotherm. Res. 184, 1–13. https://doi.org/10.1016/j.jvolgeores.2008.12.001.

Lague, D., Hovius, N., Davy, P., 2005. Discharge, discharge variability, and the bedrock channel profile. J. Geophys. Res. 110, F0406. https://doi.org/10.1029/2004JF000259.

Lague, D., 2014. The stream power river incision model: evidence, theory and beyond. Earth Surf. Process. Landforms 39, 38–61. https://doi.org/10.1002/esp.3462.

Mairine, P., Bachèlery, P., 1997. Major erosional period in the building of Piton de la Fournaise (Réunion Island). C. R. Acad. Sci. 325, 243–249.

Marder, E., Gallen, S.F., 2023. Climate control on the relationship between erosion rate and fluvial topography. Geology 51 (5), 424–427. https://doi.org/10.1130/G50832.1.

Mark, R.K., Moore, J.G., 1987. Slopes of the Hawaiian ridge. Volcanism Volume 1, 101–108. Chapter 3.

Mauritius Meteorological Services. Accessed November 1, 2020, http://metservice.intnet.mu/.
McDougall, I., Chamalaun, F.G., 1969. Isotopic dating and geomagnetic polarity studies on volcanic rocks from Mauritius, Indian Ocean. Geol. Soc. Am. Bull. 80, 1419–1442.
McDougall, I., Watkins, N.D., 1973. Age and duration of the Réunion geomagnetic polarity event. Earth Planet. Sci. Lett. 19, 443–452. https://doi.org/10.1016/0012-821X(73)90188-X.
McDougall, I., 1964. Potassium-argon ages from lavas of the Hawaiian Islands. Geol. Soc. Am. Bull. 75, 107–128. https://doi.org/10.1130/0016-7606(1964)75[107:PAFLOT]2.0.CO;2.
McDougall, I., 1971. The geochronology and evolution of the young volcanic island of Réunion, Indian Ocean. Geochim. Cosmochim. Acta 35, 261–288. https://doi.org/10.1016/0016-7037(71)90037-8.
McDougall, I., 1979. Age of shield-building volcanism of Kauai and linear migration of volcanism in the Hawaiian island chain. Earth Planet. Sci. Lett. 46, 31–42. https://doi.org/10.1016/0012-821X(79)90063-3.
Merle, O., Mairine, P., Michon, L., Bachèlery, P., Smietana, M., 2010. Calderas, landslides and paleo-canyons on Piton de la Fournaise volcano (La Réunion Island, Indian Ocean). J. Volcanol. Geotherm. Res. 189, 131–142. https://doi.org/10.1016/j.jvolgeores.2009.11.001.
Molnar, P., England, P., 1990. Late Cenozoic uplift of mountain ranges and global climate change: chicken or egg? Nature 346, 29–34. https://doi.org/10.1038/346029a0.
Molnar, P., Anderson, R.S., Kier, G., Rose, J., 2006. Relationships among probability distributions of stream discharges in floods, climate, bed load transport, and river incision. J. Geophys. Res. 111, F02001. https://doi.org/10.1029/2005JF000310.
Montaggioni, L.F., Martin-Garin, B., 2020. Episodic coral growth events during the building of Réunion and Mauritius shield volcanoes (Western Indian Ocean). Facies 66, 13. https://doi.org/10.1007/s10347-020-00597-7.
Moore, J., White, W.M., Paul, D., Duncan, R.A., Abouchami, W., Galer, S.J.G., 2011. Evolution of shield-building and rejuvenescent volcanism of Mauritius. J. Volcanol. Geotherm. Res. 207, 47–66. https://doi.org/10.1016/j.jvolgeores.2011.07.005.
Moore, J.G., 1987. Subsidence of the Hawaiian Ridge. In: Volcanism, Volume 1. U.S. Geological Survey Professional Paper 1350, Hawaii, pp. 85–100. Chapter 2.
Murphy, B.P., Johnson, J.P.L., Gasparini, N.M., Sklar, L.S., 2016. Chemical weathering as a mechanism for the climatic control of bedrock river incision. Nature 532, 223–227. https://doi.org/10.1038/nature17449.
Ollier, C., 1988. Volcanoes. Blackwell, Oxford, p. 228.
Perroud, B., 1982. Etude Volcano-Structurale Des îles Maurice Et Rodrigue (Océan Indien occidental) : Origine Du volcanisme. Volcanologie. Université scientifique et médicale de Grenoble, p. 136. Ph.D. Thesis.
Quidelleur, X., Famin, V., 2024. Last 150 kyr volcanic activity on Mauritius island (Indian ocean) revealed by new Cassignol-Gillot unspiked K–Ar ages. Quat. Geochronol. 82, 101534. https://doi.org/10.1016/j.quageo.2024.101534.
Réchou, A., Florès, O., Jumaux, G., Duflot, V., Bousquet, O., Pouppeville, C., Bonnardot, F., 2019. Spatio-temporal variability of rainfall in a high tropical island: patterns and large-scale drivers in Réunion Island. Q. J. R. Meteorolog. Soc. 145 (720), 893–909. https://doi.org/10.1002/qj.3485.
Raja, N.B., Aydin, O., 2019. Trend analysis of annual precipitation of Mauritius for the period 1981–2010. Meteorol. Atmos. Phys. 131, 789–805. https://doi.org/10.1007/s00703-018-0604-7.
Reiners, P.W., Nelson, B.K., Izuka, S.K., 1999. Structural and petrologic evolution of the Lihue basin and eastern Kauai. Hawaii. Geol. Soc. Am. Bull. 111, 674–685. https://doi.org/10.1130/0016-7606(1999)111<0674:SAPEOT>2.3.CO;2.
Rossi, M.W., Whipple, K.X., Vivoni, E.R., 2016. Precipitation and evapotranspiration controls on daily runoff variability in the contiguous United States and Puerto Rico. J. Geophys. Res. Earth Surf. 121, 128–145. https://doi.org/10.1002/2015JF003446.
Royden, L., Taylor Perron, J., 2013. Solutions of the stream power equation and application to the evolution of river longitudinal profiles. J. Geophys. Res. Earth Surf. 118 (2), 497–518. https://doi.org/10.1002/jgrf.20031.
Salvany, T., Lahitte, P., Nativel, P., Gillot, P.-Y., 2012. Geomorphic evolution of the Piton des Neiges volcano (Réunion Island, Indian Ocean): competition between volcanic construction and erosion since 1.4 Ma. Geomorphology 136, 132–147. https://doi.org/10.1016/j.geomorph.2011.06.009.
Salvany, T., 2009. Evolution morphostructurale de volcans boucliers intraplaques océaniques: Exemple des volcans de l'île de la Réunion (Océan Indien) Thèse de l'université Paris Sud (in French).
Schwanghart, W., Scherler, D., 2014. TopoToolbox 2 – MATLAB-based software for topographic analysis and modeling in Earth surface sciences. Earth Surf. Dynam. 2, 1–7. https://doi.org/10.5194/esurf-2-2-2014.
Seidl, M.A., Dietrich, W.E., Kirchner, J.W., 1994. Longitudinal profile development into bedrock: an analysis of hawaiian channels. J. Geol. 102, 457–474. https://doi.org/10.1086/629686.
Sherrod, D.R., Izuka, S.K., Cousens, B.L., 2015. Onset of rejuvenated-stage volcanism and the formation of Līhu'e Basin. In Hawaiian Volcanoes (eds R. Carey, V. Cayol, M. Poland and D. Weis). https://doi.org/10.1002/9781118872079.ch6.
Snyder, N.P., Whipple, K.X., Tucker, G.E., Merritts, D.J., 2000. Landscape response to tectonic forcing: digital elevation model analysis of stream profiles in the Mendocino triple junction region, northern California. Geol. Soc. Am. Bull. 112 (8). https://doi.org/10.1130/0016-7606(2000)112<1250:LRTTFD>2.3.CO;2.
Tucker, G.E., 2004. Drainage basin sensitivity to tectonic and climatic forcing: implications of a stochastic model for the role of entrainment and erosion thresholds. Earth Surf. Processes Landforms 29 (2), 185–205. https://doi.org/10.1002/esp.1020.
Valdes, P.J., Armstrong, E., Badger, M.P.S., Bradshaw, C.D., Bragg, F., Crucifix, M., Davies-Barnard, T., Day, J.J., Farnsworth, A., Gordon, C., Hopcroft, P.O., Kennedy, A.T., Lord, N.S., Lunt, D.J., Marzocchi, A., Parry, L.M., Pope, V., Roberts, W.H.G., Stone, E.J., Tourte, G.J.L., Williams, J.H.T., 2017. The BRIDGE HadCM3 family of climate models: hadCM3@Bristol v1.0, Geosci. Model Dev 10, 3715–3743. https://doi.org/10.5194/gmd-10-3715-2017.
Whipple, K.X., Forte, A.M., DiBiase, R.A., Gasparini, N.M., Ouimet, W.B., 2017. Timescales of landscape response to divide migration and drainage capture: implications for the role of divide mobility in landscape evolution. J. Geophys. Res. Earth Surf. 122, 248–273. https://doi.org/10.1002/2016JF003973.
Whipple, K.X., 2004. Bedrock rivers and the geomorphology of active orogens. Annu. Rev. Earth Planet. Sci. 32, 151–185. https://doi.org/10.1146/annurev.earth.32.101802.120356.
Wobus, C., Whipple, K.X., Kirby, E., Snyder, N., Johnson, J., Spyropolou, K., Crosby, B. and Sheehan, D., 2006. Tectonics from topography: procedures, promise, and pitfalls. In: Tectonics Climate Landscape Evol., Willett, S.D., Hovius, N., Brandon, M. T., Fishe, D.M. https://doi.org/10.1130/2006.2398(04).